Nanoscale Advances

ROYAL SOCIETY OF CHEMISTRY

COMMUNICATION

View Article Online
View Journal | View Issue

Cite this: *Nanoscale Adv.*, 2021, **3**, 1910

Received 28th November 2020
Accepted 12th February 2021

DOI: 10.1039/d0na01000f

rsc.li/nanoscale-advances

Theoretical study of the influence of doped niobium on the electronic properties of $CsPbBr_3$

Xingyou Liang,[a] Xuefeng Ren, *[c] Shuzhang Yang,[d] Lizhao Liu,*[b] Wei Xiong,[f] Li Cheng,[b] Tingli Ma [de] and Anmin Liu *[a]

In the family of inorganic perovskite solar cells (PSCs), $CsPbBr_3$ has attracted widespread attention due to its excellent stability under high humidity and high temperature conditions. However, power conversion efficiency (PCE) improvement of $CsPbBr_3$-based PSCs is markedly limited by the large optical absorption loss coming from the wide band gap and serious charge recombination at interfaces and/or within the perovskite film. In this work, using density functional theory calculations, we systemically studied the electronic properties of niobium (Nb)-doped $CsPbBr_3$ with different concentration ratios. As a result, it is found that doped $CsPbBr_3$ compounds are metallic at high Nb doping concentration but semiconducting at low Nb doping concentration. The calculated electronic density of states shows that the conduction band is predominantly constructed of doped Nb. These characteristics make them very suitable for solar cell and energy storage applications.

1. Introduction

Organic–inorganic hybrid perovskite solar cells (PSCs) have favourable properties including appropriate band gap, high absorption coefficient, low cost and easy fabrication process, and show great potential for photovoltaic devices.[1–6] Their power conversion efficiency (PCE) has been increased dramatically from 3.8% to a certified 25.5% by various strategies such as composition engineering, interface engineering, construction engineering, and preparation techniques.[7–14] Although the rapid increase of PCE has been realized, the intrinsic stability of hybrid perovskites under high humidity and high temperature is still a key issue for meeting the commercial requirements.[15,16]

To reduce the instability issues, the use of all-inorganic cesium lead halides ($CsPbX_3$), which contain inorganic cesium (Cs) rather than organic cations as in organic–inorganic perovskites, has been demonstrated to be an effective strategy for improving the stability of PSCs.[17–19] Thus, currently, $CsPbX_3$ has attracted much attention. It is divided into different components by tuning the halide anions, mainly focusing on $CsPbI_3$,[20,21] $CsPbI_2Br$,[22,23] $CsPbIBr_2$,[24,25] and $CsPbBr_3$.[26,27] From the family of all-inorganic PSCs, $CsPbBr_3$ exhibits superior stability under high humidity and high temperature conditions, which is significant to the practical application of PSC devices. However, the PCE is limited by large optical absorption loss and serious charge recombination. At present, the best PCE of $CsPbBr_3$-based PSCs is just around 11%.[28] Therefore, it is urgent to know how to improve the PCE and reduce the cost of $CsPbBr_3$ PSCs.

To date, several strategies have been applied to enhance the PCE and simultaneously prolong the thermal stability of inorganic PSCs. For example, Chu and co-workers fabricated an amorphous Nb_2O_5 film as the ETL of inorganic planar $CsPbBr_3$ by the magnetron sputtering method, and 5.74% PCE was obtained due to the suitable surface work function and high transmittance of amorphous Nb_2O_5 and low charge recombination at the amorphous $Nb_2O_5/CsPbBr_3$ interface.[29] Yu *et al.* demonstrated an interesting method by face-down liquid-space restriction to prepare high-quality $CsPbBr_3$ perovskite films on compact TiO_2 layers. This novel method can obtain uniform, smooth and high-quality perovskite films, which greatly increased the PCE and V_{oc} in planar all-inorganic $CsPbBr_3$ PSCs.[30] Zhong *et al.* developed a one-step solution-processing method to fabricate $CsPbBr_3$ films using precursor engineering

[a]State Key Laboratory of Fine Chemicals, School of Chemical Engineering, Dalian University of Technology, China. E-mail: anmin0127@163.com; liuanmin@dlut.edu.cn

[b]Key Laboratory of Materials Modification by Laser, Ion and Electron Beams (Dalian University of Technology), Ministry of Education, Dalian 116024, China. E-mail: lizhao_liu@dlut.edu.cn

[c]School of Ocean Science and Technology, Dalian University of Technology, Panjin, 124221, China. E-mail: renxuefeng@dlut.edu.cn

[d]Graduate School of Life Science and Systems Engineering, Kyushu Institute of Technology, 2-4 Hibikino, Wakamatsu, Kitakyushu, Fukuoka 808-0196, Japan

[e]Department of Materials Science and Engineering, China Jiliang University, Hangzhou, 310018, China

[f]Key Laboratory of Industrial Ecology and Environmental Engineering (Ministry of Education), School of Environmental Sciences and Technology, Dalian University of Technology, Dalian 116024, China

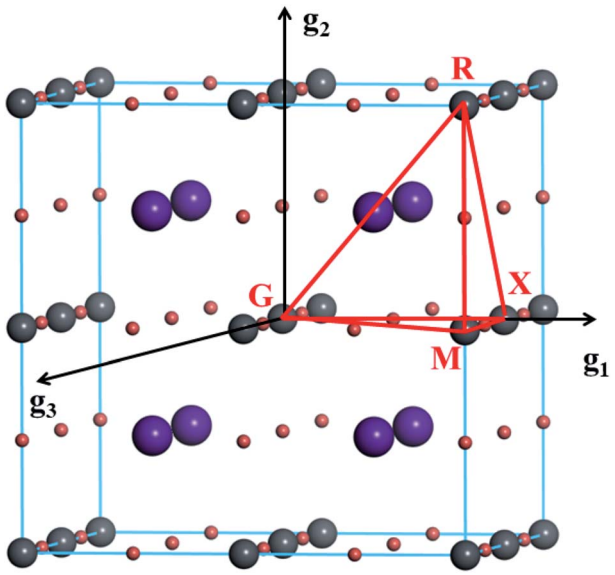

Fig. 1 Visualization of k-point paths in the 1st Brillouin zone; $\mathbf{g}_1$, $\mathbf{g}_2$, and $\mathbf{g}_3$ are vectors for the reciprocal lattice.

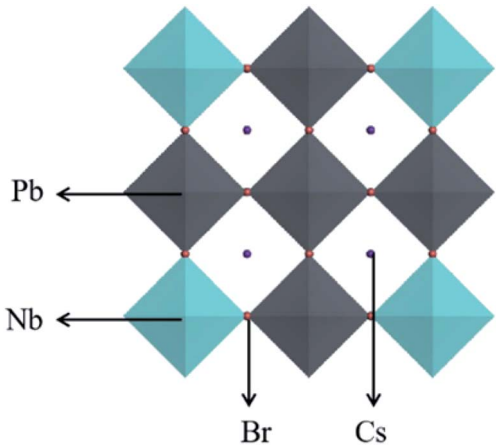

Fig. 2 Schematic diagram of the crystal structure of Nb-doped $CsPbBr_3$.

and applied it for a $CsPbBr_3$-based device. A PCE of 7.37% has been achieved with high stability over 1500 h under an ambient atmosphere with 30–35% relative humidity.[31] Liao *et al.* developed a modified multistep spin-coating strategy for $CsPbBr_3$ film preparation, and the optimized PCE was improved to 8.12%. This might be mainly attributed to the high crystallinity and reduced density of trap states of the $CsPbBr_3$ film.[32] They also selected a novel antisolvent-washing strategy for highly efficient carbon-based $CsPbBr_3$ PSCs, increasing the PCE to 8.55%.[33] Tang *et al.* reported a Lewis-base polymer, polyvinyl acetate (PVAc), to modify the $CsPbBr_3$ film. A maximum PCE of up to 9.53% with an excellent V_{oc} of 1.553 V was achieved for the $CsPbBr_3$-based PSC.[34] Yang *et al.* applied a vapor-assisted solution technique to prepare a uniform and pure $CsPbBr_3$ film. The optimized $CsPbBr_3$ PSC showed a PCE of 10.45% and outstanding stability for over 90 days under harsh conditions (80% RH, 85 °C).[35] Qi *et al.* proposed a phase transition-induced method to produce high-quality $CsPbBr_3$ thin films. A PCE of 10.91% was obtained for n–i–p structured PSCs with metal electrodes, and the carbon electrode-based devices exhibited excellent long-term stability and retained 80% of the initial efficiency in ambient air for more than 2000 h without any encapsulation.[28]

Although there are many ways to improve the efficiency of the device, few studies were reported to fundamentally improve the absorption capacity of this kind of material, and the current efficiency is far from its ultimate efficiency. Theoretical calculations are an effective method to design materials and study the mechanism.[36–40]

In this study, we systematically study the electronic properties of niobium (Nb)-doped $CsPbBr_3$ with different concentration ratios using first-principles calculations. This work will provide a good theoretical basis for understanding the structure and electronic properties of these compounds. Through the analysis of these results, we propose that Nb-doped $CsPbBr_3$ may be a promising solar cell absorber with good band gap and light absorption properties, which provides a feasible method for improving the efficiency of the device.

2. DFT calculation details

The Vienna *Ab initio* Simulation Package (VASP) based on the plane-wave pseudopotential technique was employed, using the Perdew–Burke–Ernzerhof (PBE) functional for the exchange-correlation interaction and the projector augmented wave (PAW) pseudopotential for the ion–electron interaction.[41–44] A kinetic energy cutoff of 350 eV was chosen to ensure good convergence of the total energy and stress. The well-tested Monkhorst–Pack k grid of a uniform spacing of 0.02 $Å^{-1}$ was adopted to sample the first Brillouin zone. All the structures were fully relaxed using the conjugate gradient algorithm until the force on each atom was less than 0.001 eV $Å^{-1}$ and the energy was converged to 10^{-4} eV.

We calculate the doping energy (E_{doping}) of five kinds of supercell structures doped with $CsPbBr_3$ at different Nb concentrations, and the formula of E_{doping} is given by

$$E_{doping} = E_{dop} + E_{Pb} - E_{pure} - E_{Nb} \quad (1)$$

where E_{dop} is the total energy of the system after $CsPbBr_3$ is doped with Nb atoms, E_{pure} is the total energy of the pure

Table 1 Supercells and chemical formulae of different concentration ratios of Nb doped in $CsPbBr_3$

Supercell	Chemical formula	Doping concentration
2 × 1 × 1	Br_6NbCs_2Pb	50%
2 × 2 × 1	$Br_{12}NbCs_4Pb_3$	25%
2 × 2 × 2	$Br_{24}NbCs_8Pb_7$	12.5%
2 × 2 × 4	$Br_{48}NbCs_{16}Pb_{15}$	6.25%
2 × 4 × 4	$Br_{96}NbCs_{32}Pb_{31}$	3.125%

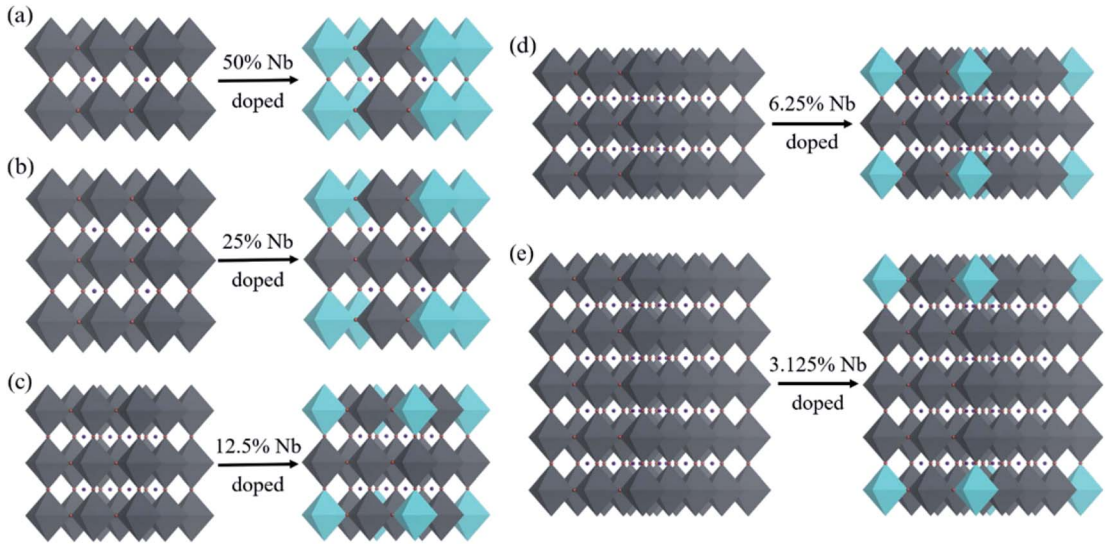

Fig. 3 Schematic diagrams of the pristine and Nb-doped $CsPbBr_3$ crystal structures with different concentration ratios.

Table 2 The raw data for calculating the doping energy

Structures	Pristine (eV)	Doped (eV)
2 × 1 × 1 supercell	−31.7945	−35.2799
2 × 2 × 1 supercell	−63.5882	−66.9168
2 × 2 × 2 supercell	−127.177	−130.491
2 × 2 × 4 supercell	−254.354	−257.757
2 × 4 × 4 supercell	−508.72	−512.19
Pb atom	−0.095720351	
Nb atom	−0.64194424	

undoped $CsPbBr_3$ system, and E_{Pb} and E_{Nb} are the energy of single atoms of Pb and Nb, respectively. Visualization of *k*-point paths in the 1st Brillouin zone is shown in Fig. 1.

3. Results and discussion

In order to explore the effect of Nb doping of $CsPbBr_3$ on its absorption capacity, we doped Nb into $CsPbBr_3$ by expanding cells, that is, doping one Nb atom in each supercell, as shown in Fig. 2. We constructed Nb-doped $CsPbBr_3$ with 50%, 25%, 12.5%, 6.25%, and 3.125% concentration ratios, and the corresponding supercells and chemical formulae are shown in Table 1. The original $CsPbBr_3$ structure of five different supercells and the crystal structure after doping with different Nb concentrations are shown in Fig. 3.

The raw data used to calculate the doping energy are shown in Table 2. According to formula (1), we calculated the doping energies of Nb atoms doped in five supercell structures. The detailed calculation results are shown in Table 3. The results show that as the doping concentration increases, the doping energy gradually increases. When the doping concentration of Nb reaches 12.5%, the doping energy reaches the maximum value of −2.77 eV. However, when the doping concentration of Nb atoms is increased, the doping energy will gradually decrease.

The optimization results of lattice parameters for these pristine and differently Nb doped $CsPbBr_3$ are shown in Table 4. Since Nb is significantly smaller than the atomic radius of Pb, when Nb is doped to replace the Pb atom in $CsPbBr_3$, the lattice constant will be significantly reduced.

Based on the relaxed structures, we studied the electronic properties of these compounds, including the band structures and density of states, which will be discussed below. Fig. 4 shows the band structures of the undoped system calculated by the PBE method and the Nb-doped system with different concentrations. Through comparison, it is found that the Fermi level of $CsPbBr_3$ after doping with Nb is closer to the conduction band. As shown in Fig. 4a, the energy band of $CsPbBr_3$ undoped with Nb shows a direct band gap. The highest point of the valence band (VBM) and the lowest point of the conduction band (CBM) are located at point R in the first Brillouin zone, respectively. Moreover, all undoped structures have the same

Table 3 Band gaps and doping energy of different concentration ratios of Nb doped in $CsPbBr_3$

Supercell	Chemical formula	Doping concentration	*k*-points	Gap (eV)	Doping energy (eV)
2 × 1 × 1	$Cs_2Pb_2Br_6$	0	4 × 8 × 8	2.51	—
2 × 1 × 1	$Cs_2PbNbBr_6$	50%	4 × 8 × 8	0 (metallic)	−2.94
2 × 2 × 1	$Cs_4Pb_3NbBr_{12}$	25%	4 × 4 × 8	0 (metallic)	−2.78
2 × 2 × 2	$Cs_8Pb_7NbBr_{24}$	12.5%	4 × 4 × 2	1.94	−2.77
2 × 2 × 4	$Cs_{16}Pb_{15}NbBr_{48}$	6.25%	4 × 4 × 2	1.89	−2.87
2 × 4 × 4	$Cs_{32}Pb_{31}NbBr_{96}$	3.125%	4 × 2 × 2	1.84	−2.92

Table 4 Comparison of calculated lattice parameters of pristine and Nb-doped $CsPbBr_3$

	Supercells									
	2 × 1 × 1		2 × 2 × 1		2 × 2 × 2		2 × 2 × 4		2 × 4 × 4	
Lattice parameters	Pristine	50% Nb doped	Pristine	25% Nb doped	Pristine	12.5% Nb doped	Pristine	6.25% Nb doped	Pristine	3.125% Nb doped
a (Å)	12.001	11.426	11.986	11.758	11.986	11.881	11.982	11.936	11.980	11.956
b (Å)	6.005	5.713	11.986	11.758	11.986	11.881	11.982	11.936	23.960	23.908
c (Å)	6.005	5.713	5.993	5.8796	11.986	11.881	23.964	23.873	23.960	23.908

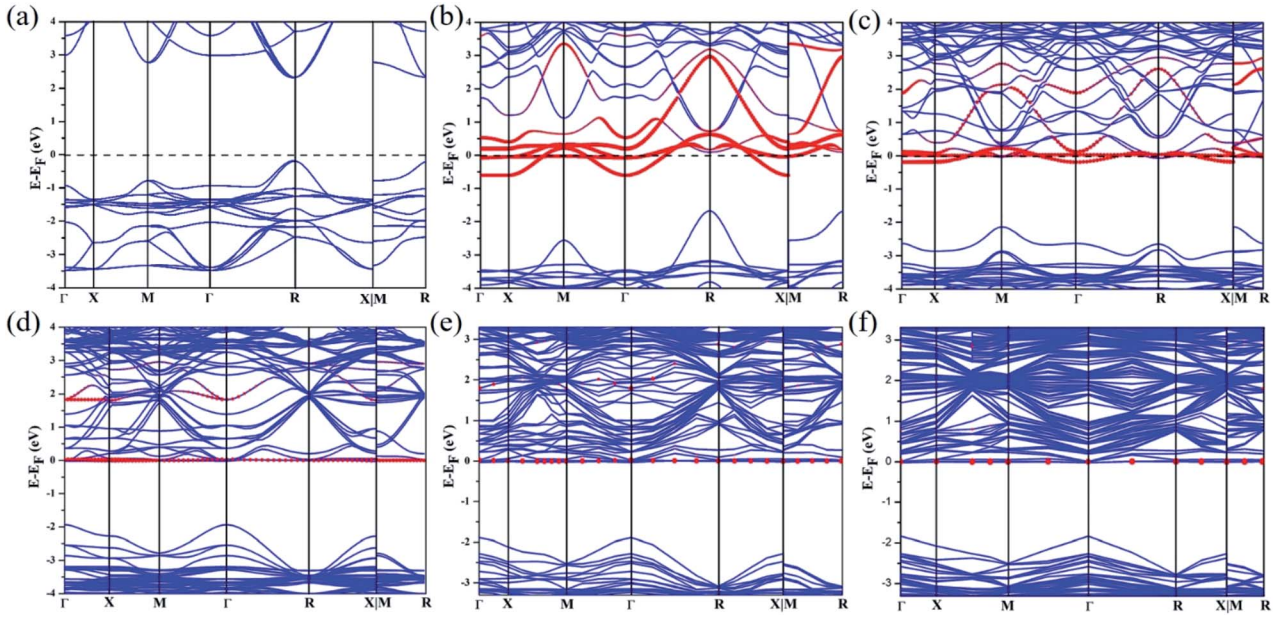

Fig. 4 (a) Band structures of the $CsPbBr_3$ supercell of 2 × 1 × 1. Band structures of different Nb doping concentration ratios of (b) 50%, (c) 25%, (d) 12.5%, (e) 6.25%, and (f) 3.125% corresponding to different pristine $CsPbBr_3$ supercells. The red bands are those of Nb.

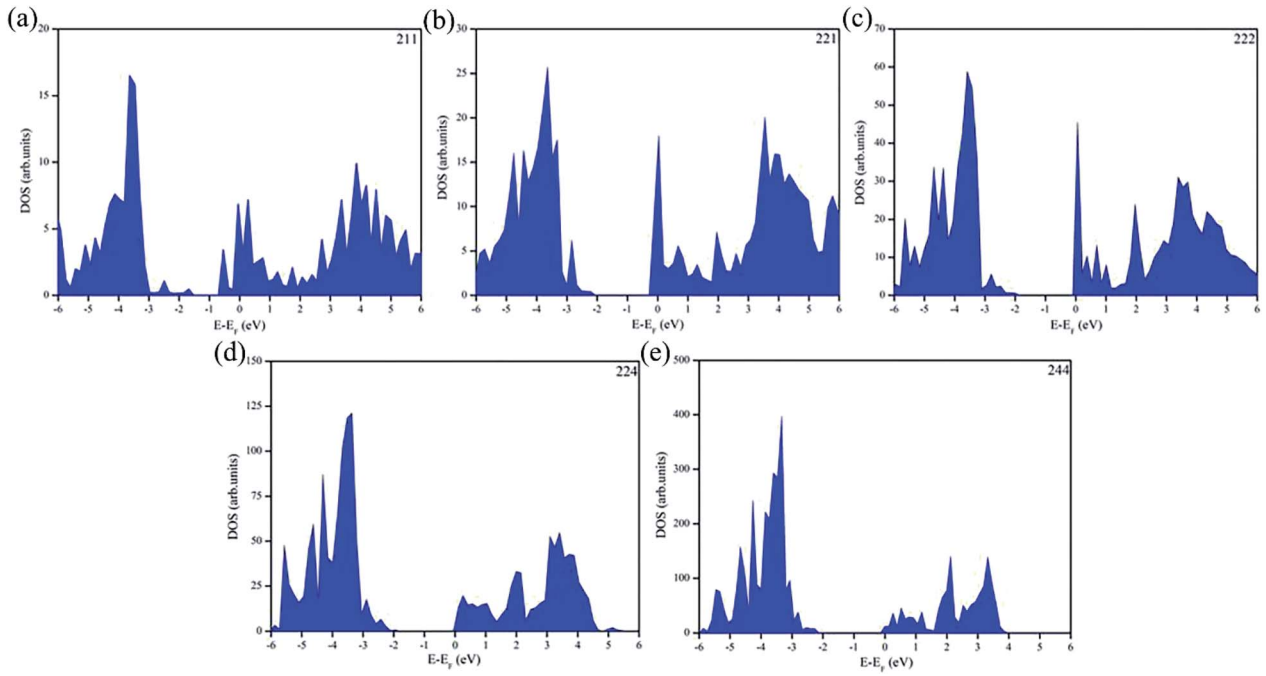

Fig. 5 Density of states (DOS) of Nb-doped $CsPbBr_3$ with different concentration ratios. (a) 50%, (b) 25%, (c) 12.5%, (d) 6.25%, and (e) 3.125%.

band gap. When the doping concentration of Nb is 50% or 25%, both structures show the properties of metals, as shown in Fig. 4b and c. Furthermore, when the doping concentration of Nb is 12.5%, 6.25% or 3.125%, the Fermi level is closer to the conduction band, which indicates an n-type semiconductor. There is a direct band gap at the Γ point, and the forbidden band widths are 1.94 eV, 1.89 eV, and 1.84 eV, which correspond to Fig. 4d, e and f, respectively.

The properties of the electronic band gap energy of different concentration ratios of Nb doping in $CsPbBr_3$ are further explained by the density of states. The density of states (DOS) explains the properties of these materials, as shown in Fig. 5. It can be clearly seen that the materials in Fig. 5a and b have crossed the Fermi level, which proves that when the doping concentration of Nb in $CsPbBr_3$ is 50% or 25%, the material becomes a metallic conductor. In Fig. 5c–e, none of them cross the Fermi level, which proves that these materials are semiconductors.

4. Conclusion

In summary, $CsPbBr_3$ is an excellent material for improving the stability of PSCs. Doping Nb into the material is considered to be an effective method to improve the PCE. Through DFT calculations, we systematically studied the electronic properties of $CsPbBr_3$ doped with different Nb concentration ratios, including the band structure and density of states. The results show that when the doping concentration of Nb is 3.125%, 6.25% or 12.5%, all three compounds have semiconductor properties, the band gaps are direct, and the basic band gaps occur at Γ symmetry points. As the doping concentration increases, the band gap width gradually increases. When the doping concentration of Nb is too high (25%, 50%), the compounds are all metallic conductors, which do not have the properties of semiconductors. From this work, we can expect that the performance of PCE and long-term stability of doped $CsPbBr_3$ at a certain Nb concentration will be greatly improved.

Conflicts of interest

The authors declare no competing interests.

Acknowledgements

Support of the National Natural Science Foundation of China (21902021, 21908017, 51972293, and 51772039), the Open Foundation of Key Laboratory of Industrial Ecology and Environmental Engineering, MOE(KLIEEE-20-01), the Fundamental Research Funds for the Central Universities (DUT20RC(4)020, DUT20RC(4)018, and DUT20LAB304), and the Supercomputing Center of Dalian University of Technology for this work is gratefully acknowledged.

References

1 M. Z. Liu, M. B. Johnston and H. J. Snaith, Efficient planar heterojunction perovskite solar cells by vapour deposition, *Nature*, 2013, **501**(7467), 395–398.
2 W. Y. Nie, H. H. Tsai, R. Asadpour, J. C. Blancon, A. J. Neukirch, G. Gupta, J. J. Crochet, M. Chhowalla, S. Tretiak, M. A. Alam, H. L. Wang and A. D. Mohite, High-efficiency solution-processed perovskite solar cells with millimeter-scale grains, *Science*, 2015, **347**(6221), 522–525.
3 N. J. Jeon, J. H. Noh, Y. C. Kim, W. S. Yang, S. Ryu and S. I. Seok, Solvent engineering for high-performance inorganic–organic hybrid perovskite solar cells, *Nat. Mater.*, 2014, **13**(9), 897–903.
4 S. D. Stranks, P. K. Nayak, W. Zhang, T. Stergiopoulos and H. J. Snaith, Formation of Thin Films of Organic–Inorganic Perovskites for High-Efficiency Solar Cells, *Angew. Chem., Int. Ed.*, 2015, **54**(11), 3240–3248.
5 W. J. Yin, J. H. Yang, J. Kang, Y. F. Yan and S. H. Wei, Halide perovskite materials for solar cells: a theoretical review, *J. Mater. Chem. A*, 2015, **3**(17), 8926–8942.
6 L. Meng, J. B. You, T. F. Guo and Y. Yang, Recent Advances in the Inverted Planar Structure of Perovskite Solar Cells, *Acc. Chem. Res.*, 2016, **49**(1), 155–165.
7 A. Kojima, K. Teshima, Y. Shirai and T. Miyasaka, Organometal Halide Perovskites as Visible-Light Sensitizers for Photovoltaic Cells, *J. Am. Chem. Soc.*, 2009, **131**(17), 6050–6051.
8 Laboratory, N. R. E., *Best Research-Cell Efficiency Chart*. 2020.
9 P. Kumar and A. K. Chauhan, Highly efficient flexible perovskite solar cells and their photo-stability, *J. Phys. D: Appl. Phys.*, 2020, **53**(3), 035101.
10 Y. H. Xu, C. Gao, S. W. Tang, J. Zhang, Y. Q. Chen, Y. J. Zhu and Z. Y. Hu, Comprehensive understanding of $TiCl_4$ treatment on the compact TiO_2 layer in planar perovskite solar cells with efficiencies over 20%, *J. Alloys Compd.*, 2019, **787**, 1082–1088.
11 D. S. Mann, Y. H. Seo, S. N. Kwon and S. I. Na, Efficient and stable planar perovskite solar cells with a PEDOT:PSS/SrGO hole interfacial layer, *J. Alloys Compd.*, 2020, 812.
12 E. Gonzalez-Juarez, D. Gonzalez-Quijano, D. F. Garcia-Gutierrez, D. I. Garcia-Gutierrez, J. Ibarra-Rodriguez and E. Sanchez, Improving performance of perovskites solar cells using solvent engineering, *via* Lewis adduct of MAI-DMSO-PbI_2 and incorporation of imidazolium cation, *J. Alloys Compd.*, 2020, 817.
13 T. T. Ngo, S. Masi, P. F. Mendez, M. Kazes, D. Oron and I. M. Sero, PbS quantum dots as additives in methylammonium halide perovskite solar cells: the effect of quantum dot capping, *Nanoscale Adv.*, 2019, **1**(10), 4109–4118.
14 Z. Liu, S. Z. Wu, X. J. Yang, Y. J. Zhou, J. R. Jin, J. M. Sun, L. Zhao and S. M. Wang, The dual interfacial modification of 2D g-C_3N_4 for high-efficiency and stable planar perovskite solar cells, *Nanoscale Adv.*, 2020, **2**(11), 5396–5402.
15 S. Z. Yang, X. Z. Song, L. G. Gao, N. Wang, X. G. Ding, S. F. Wang and T. L. Ma, Seamless Interfacial Formation by Solution-Processed Amorphous Hydroxide Semiconductor for Highly Efficient Electron Transport, *ACS Appl. Energy Mater.*, 2018, **1**(9), 4564–4571.

16 Y. Wang, T. Y. Zhang, F. Xu, Y. H. Li and Y. X. Zhao, A Facile Low Temperature Fabrication of High Performance $CsPbI_2Br$ All-Inorganic Perovskite Solar Cells, *Sol. RRL*, 2018, **2**(1), 1700180.

17 J. R. Zhang, G. Hodes, Z. W. Jin and S. Z. Liu, All-Inorganic $CsPbX_3$ Perovskite Solar Cells: Progress and Prospects, *Angew. Chem., Int. Ed.*, 2019, **58**(44), 15596–15618.

18 S. Liu, Y. J. Guan, Y. S. Sheng, Y. Hu, Y. G. Rong, A. Y. Mei and H. W. Han, A Review on Additives for Halide Perovskite Solar Cells, *Adv. Energy Mater.*, 2020, **10**(13), 1902492.

19 G. Q. Tong, L. K. Ono and Y. B. Qi, Recent Progress of All-Bromide Inorganic Perovskite Solar Cells, *Energy Technol.*, 2020, **8**(4), 1900961.

20 P. Y. Wang, X. W. Zhang, Y. Q. Zhou, Q. Jiang, Q. F. Ye, Z. M. Chu, X. X. Li, X. L. Yang, Z. G. Yin and J. B. You, Solvent-controlled growth of inorganic perovskite films in dry environment for efficient and stable solar cells, *Nat. Commun.*, 2018, **9**, 2225.

21 G. E. Eperon, G. M. Paterno, R. J. Sutton, A. Zampetti, A. A. Haghighirad, F. Cacialli and H. J. Snaith, Inorganic caesium lead iodide perovskite solar cells, *J. Mater. Chem. A*, 2015, **3**(39), 19688–19695.

22 C. Liu, W. Z. Li, C. L. Zhang, Y. P. Ma, J. D. Fan and Y. H. Mai, All-Inorganic $CsPbI_2Br$ Perovskite Solar Cells with High Efficiency Exceeding 13%, *J. Am. Chem. Soc.*, 2018, **140**(11), 3825–3828.

23 L. Yan, Q. F. Xue, M. Y. Liu, Z. L. Zhu, J. J. Tian, Z. C. Li, Z. Chen, Z. M. Chen, H. Yan, H. L. Yip and Y. Cao, Interface Engineering for All-Inorganic $CsPbI_2Br$ Perovskite Solar Cells with Efficiency over 14%, *Adv. Mater.*, 2018, **30**(33), 1802509.

24 S. Z. Yang, Z. L. Guo, L. G. Gao, F. Y. Yu, C. Zhang, M. Q. Fan, G. Y. Wei and T. L. Ma, Bifunctional Dye Molecule in All-Inorganic $CsPbIBr_2$ Perovskite Solar Cells with Efficiency Exceeding 10%, *Sol. RRL*, 2019, **3**(9), 1900212.

25 C. Liu, W. Z. Li, J. H. Chen, J. D. Fan, Y. H. Mai and R. E. I. Schropp, Ultra-thin MoO_x as cathode buffer layer for the improvement of all-inorganic $CsPbIBr_2$ perovskite solar cells, *Nano Energy*, 2017, **41**, 75–83.

26 J. L. Duan, Y. Y. Zhao, B. L. He and Q. W. Tang, High-Purity Inorganic Perovskite Films for Solar Cells with 9.72% Efficiency, *Angew. Chem., Int. Ed.*, 2018, **57**(14), 3787–3791.

27 J. L. Duan, Y. Y. Zhao, X. Y. Yang, Y. D. Wang, B. L. He and Q. W. Tang, Lanthanide Ions Doped $CsPbBr_3$ Halides for HTM-Free 10.14%-Efficiency Inorganic Perovskite Solar Cell with an Ultrahigh Open-Circuit Voltage of 1.594 V, *Adv. Energy Mater.*, 2018, **8**(31), 1802346.

28 G. Q. Tong, T. T. Chen, H. Li, L. B. Qiu, Z. H. Liu, Y. Y. Dang, W. T. Song, L. K. Ono, Y. Jiang and Y. B. Qi, Phase transition induced recrystallization and low surface potential barrier leading to 10.91%-efficient $CsPbBr_3$ perovskite solar cells, *Nano Energy*, 2019, **65**, 104015.

29 F. Zhao, Y. X. Guo, X. Wang, J. H. Tao, J. C. Jiang, Z. G. Hu and J. H. Chu, Enhanced performance of carbon-based planar $CsPbBr_3$ perovskite solar cells with room-temperature sputtered Nb_2O_5 electron transport layer, *Sol. Energy*, 2019, **191**, 263–271.

30 P. P. Teng, X. P. Han, J. W. Li, Y. Xu, L. Kang, Y. R. Q. Wang, Y. Yang and T. Yu, Elegant Face-Down Liquid-Space-Restricted Deposition of $CsPbBr_3$ Films for Efficient Carbon-Based All-Inorganic Planar Perovskite Solar Cells, *ACS Appl. Mater. Interfaces*, 2018, **10**(11), 9541–9546.

31 D. W. Huang, P. F. Xie, Z. X. Pan, H. S. Rao and X. H. Zhong, One-step solution deposition of $CsPbBr_3$ based on precursor engineering for efficient all-inorganic perovskite solar cells, *J. Mater. Chem. A*, 2019, **7**(39), 22420–22428.

32 X. Y. Liu, X. H. Tan, Z. Y. Liu, H. B. Ye, B. Sun, T. L. Shi, Z. R. Tang and G. L. Liao, Boosting the efficiency of carbon-based planar $CsPbBr_3$ perovskite solar cells by a modified multistep spin-coating technique and interface engineering, *Nano Energy*, 2019, **56**, 184–195.

33 X. Y. Liu, Z. Y. Liu, X. H. Tan, H. B. Ye, B. Sun, S. Xi, T. L. Shi, Z. R. Tang and G. L. Liao, Novel antisolvent-washing strategy for highly efficient carbon-based planar $CsPbBr_3$ perovskite solar cells, *J. Power Sources*, 2019, **439**, 227092.

34 Y. Ding, B. L. He, J. W. Zhu, W. Y. Zhang, G. D. Su, J. L. Duan, Y. Y. Zhao, H. Y. Chen and Q. W. Tang, Advanced Modification of Perovskite Surfaces for Defect Passivation and Efficient Charge Extraction in Air-Stable $CsPbBr_3$ Perovskite Solar Cells, *ACS Sustainable Chem. Eng.*, 2019, **7**(23), 19286–19294.

35 X. Li, Y. Tan, H. Lai, S. P. Li, Y. Chen, S. W. Li, P. Xu and J. Y. Yang, All-Inorganic $CsPbBr_3$ Perovskite Solar Cells with 10.45% Efficiency by Evaporation-Assisted Deposition and Setting Intermediate Energy Levels, *ACS Appl. Mater. Interfaces*, 2019, **11**(33), 29746–29752.

36 Y.-F. Ding, Z.-L. Yu, P.-B. He, Q. Wan, B. Liu, J.-L. Yang and M.-Q. Cai, High-performance Photodetector Based on InSe/$Cs_2XI_2Cl_2$ (X = Pb, Sn, and Ge) Heterostructures, *Phys. Rev. Appl.*, 2020, **13**(6), 064053.

37 L.-Y. Pan, Y.-F. Ding, Z.-L. Yu, Q. Wan, B. Liu and M.-Q. Cai, Layer-dependent optoelectronic property for all-inorganic two-dimensional mixed halide perovskite $Cs_2PbI_2Cl_2$ with a Ruddlesden-Popper structure, *J. Power Sources*, 2020, 451.

38 T. Ruan, B. Wang, Y. Yang, X. Zhang, R. Song, Y. Ning, Z. Wang, H. Yu, Y. Zhou, D. Wang, H. Liu and S. Dou, Interfacial and Electronic Modulation *via* Localized Sulfurization for Boosting Lithium Storage Kinetics, *Adv. Mater.*, 2020, **32**(17), 2000151.

39 D.-N. Yan, C.-S. Liao, Y.-Q. Zhao, B. Liu, J.-L. Yang and M.-Q. Cai, Theoretical prediction of double perovskite $Cs_2Ag_xCu_{1-x}In_yTb_{1-y}Cl_6$ for infrared detection, *J. Phys. D: Appl. Phys.*, 2020, **53**(26), 265302.

40 B. Wang, T. Liu, A. Liu, G. Liu, L. Wang, T. Gao, D. Wang and X. S. Zhao, A Hierarchical Porous C@$LiFePO_4$/Carbon Nanotubes Microsphere Composite for High-Rate Lithium-Ion Batteries: Combined Experimental and Theoretical Study, *Adv. Energy Mater.*, 2016, **6**(16), 1600426.

41 G. Kresse and J. Furthmuller, Efficiency of *ab initio* total energy calculations for metals and semiconductors using a plane-wave basis set, *Comput. Mater. Sci.*, 1996, **6**(1), 15–50.

42 J. P. Perdew, K. Burke and M. Ernzerhof, Generalized gradient approximation made simple, *Phys. Rev. Lett.*, 1996, **77**(18), 3865–3868.
43 P. E. Blochl, Projector Augmented-Wave Method, *Phys. Rev. B: Condens. Matter Mater. Phys.*, 1994, **50**(24), 17953–17979.
44 G. Kresse and D. Joubert, From ultrasoft pseudopotentials to the projector augmented-wave method, *Phys. Rev. B: Condens. Matter Mater. Phys.*, 1999, **59**(3), 1758–1775.